

Generation of phonons from electrostriction in small-core optical waveguides

Vincent Laude^{1, a)} and Jean-Charles Beugnot^{1, b)}

*Institut FEMTO-ST, Université de Franche-Comté, CNRS UMR 6174,
F-25044 Besançon cedex, France*

We investigate the generation of acoustic phonons from electrostriction of optical waves in small core waveguides. We specifically consider simple step-index strip waveguides composed of silica or silicon in air, with sub-micron lateral dimensions. Such waveguides support one or a few optical modes, but a rich spectrum of acoustic phonons that becomes densely populated as the phonon frequency increases. We evaluate rigorously the phonon energy density that results from the electrostriction of two frequency detuned guided optical waves, that are either co- or contra-propagating, including phonon loss. Plotting this energy density as a function of frequency detuning reveals the phonon wave packets that are electrostrictively active and gives a quantitative estimation of the energy transfer from optical waves to particular phonons. Furthermore, in the backward interaction geometry, the dispersion relation of such phonons can be accessed directly by varying the optical wavelength.

PACS numbers: 43.20.+g, 43.40.+s, 46.40.Cd, 63.20.-e

^{a)}Electronic mail: vincent.laude@femto-st.fr

^{b)}Electronic mail: jc.beugnot@femto-st.fr

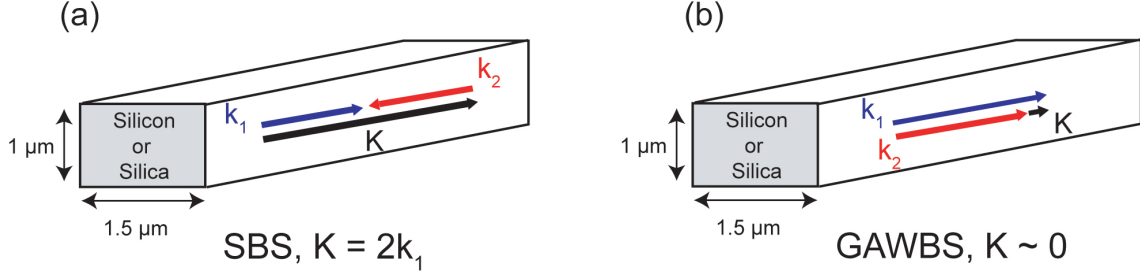


FIG. 1. Strip waveguide definition and phase-matching diagrams for (a) stimulated Brillouin (back)scattering (SBS) and (b) guided acoustic wave Brillouin scattering (GAWBS). The solid strip is composed of silicon or silica and surrounded by air.

I. INTRODUCTION

Nanostructured crystal waveguides have attracted attention recently in view of obtaining simultaneous confinement of elastic and optical waves and hence potentially strong interactions^{1,2}. Optomechanical interactions involve optical surface forces such as radiation pressure³, which are predicted to scale to large values in nanoscale waveguides⁴⁻⁶. In addition, volume optical forces are induced in microscale waveguides via electrostriction, as exemplified by Brillouin scattering effects – nonlinear processes where two photons interact with a co-propagating acoustic phonon, both generating the phonon and being scattered by it⁷. This phenomenon is broadly documented for silica optical fibers, in both theory and experiment^{8,9}. From the computation of phonon dispersion in optical fibers or waveguides, conventional stimulated Brillouin scattering (SBS) models determine the Brillouin gain spectrum from an elasto-optic overlap integral^{10,11}. The precise dynamics of the generation of phonon wave packets (or elastic waves) by optical waves through electrostriction, however, has not been treated in detail until recently¹².

In this paper, we consider the electrostriction of phonon wave packets from guided optical waves in a simple model system: the strip waveguide exemplified in Figure 1. The waveguide has a rectangular cross-section with width $1.5 \mu\text{m}$ and thickness $1 \mu\text{m}$, and is composed of a single homogeneous dielectric material surrounded by air. The dimensions were chosen to ensure single mode optical guidance at a wavelength of $1.55 \mu\text{m}$ in case the waveguide is made of silica, but the case of silicon is considered as well in order to hold a comparison. For both materials, the waveguide can be fabricated by microelectronic technologies, so

that the corresponding experiments are in principle feasible. The main objective of the paper is to expose the rich dynamics of phonon generation, even within the simplest of optical waveguides, and to obtain the energy transferred from optical waves to particular phonons and their polarization. It is found that these properties strongly depend on material properties, including the photoelastic tensor and phonon losses. Our numerical model is based on a finite element formulation of the elastodynamic wave equation subject to an arbitrary volume optical force; it is rigorous in that it naturally takes into account all anisotropic and structural details of the wave propagation problem. Significantly, there is no need to resort to a full phononic band structure computation¹³, followed by the computation of overlap integrals. In contrast, the spatial distribution of phonon wavepackets is obtained directly as a result of the applied optical force, and thus never has to be assumed to arise from a given normal elastic mode of the waveguide.

The paper is organized as follows. We first summarize the finite element elastodynamic model and then proceed to show electrostriction gain spectra for both silica and silicon strip waveguides. Such spectra show a series of Lorentzian resonances, the width of which is dictated by phonon losses, introduced in the model via a frequency-dependent viscoelastic tensor. We then proceed to discuss the effect of the dimensions of the waveguide and the differences between silica and silicon strip waveguides. The importance of the shear components of the displacements comes out of this discussion. We end by discussing the possibility of measuring phonon dispersion via all-optical means.

II. THEORY

The elastodynamic equation describing the electrostriction of acoustic phonon wavepackets is¹²

$$\rho \frac{\partial^2 u_i}{\partial t^2} - [c_{ijkl} u_{k,l}]_{,j} = [\epsilon_0 \chi_{klij} E_k E_l^*]_{,j}, \quad (1)$$

with

$$\chi_{klij} = \epsilon_{im} \epsilon_{jn} p_{klmn}. \quad (2)$$

ϵ_{ij} is the relative dielectric tensor at optical frequencies, c_{klij} is the elastic tensor, and p_{klmn} is the photoelastic tensor. Tensorial notations are used to keep expressions short and summation over repeated indices is implied. Indices placed after a comma indicate

partial derivatives are taken, e.g., $u_{k,l} = \frac{\partial u_k}{\partial x_l}$. Note that the transverse variations of the two incident optical waves are fully taken into account when defining the electrostriction stress tensor $T_{ij}^{\text{es}} = -\epsilon_0 \chi_{kl ij} E_k E_l^*$. The electrostrictive (volume) force is the divergence of the electrostriction stress tensor, $T_{ij,j}^{\text{es}}$.

Brillouin-type scattering processes are third-order parametric processes involving two photons and one phonon. Phase-matching must be achieved in order for the interaction to build constructively. For instance, a pump photon with center angular frequency ω_1 and wavenumber k_1 can produce a down-shifted Stokes photon characterized by center angular frequency ω_2 and wavenumber k_2 when scattered by an acoustic phonon of frequency $\omega = \omega_1 - \omega_2$ and wavenumber $k = k_1 - k_2$. Electrostriction of an acoustic phonon is the converse effect and is obtained from the interaction of two incident photons satisfying the previous phase-matching conditions. In this paper, we consider wave fields containing enough photons or phonons so that a classical picture can be used. The total incident optical field is the superposition of two guided monochromatic waves with frequencies ω_1 and ω_2 ,

$$E_k(r, z; t) = E_k^1(r) e^{i(\omega_1 t - k_1 z)} + E_k^2(r) e^{i(\omega_2 t - k_2 z)}, \quad (3)$$

with wavevectors $k_1 = k(\omega_1)$ and $k_2 = k(\omega_2)$ satisfying a dispersion relation for guided waves. Because we are considering acoustic phonons, ω is much smaller than ω_1 or ω_2 . Two cases can be separated in the case of optical waveguides. As depicted in Fig. 1, if the two optical waves are contra-propagative, the phase-matching conditions of stimulated Brillouin backscattering (SBS)¹⁴ are achieved, with $k_2 \approx -k_1$ and $k \approx 2k_1$. Conversely, if the two optical waves are co-propagative, the phase-matching conditions of guided acoustic wave Brillouin scattering (GAWBS)¹⁵ are achieved, with $k_2 \approx k_1$ and $k \approx 0$.

The only source term at frequency detuning $\omega = \omega_1 - \omega_2$ is proportional to $\exp(i(\omega t - kz))$ with $k = k_1(\omega_1) - k_2(\omega_2)$. Because of this source term, the following ansatz is assumed for the acoustic waves

$$u_i(r, z; t) = \bar{u}_i(r) e^{i(\omega t - kz)}, \quad (4)$$

with $\bar{u}_i(r)$ the transverse profile of the elastic phonon wave packet. We solve for the unknown displacements $\bar{u}_i(r)$ by setting k to a given value and scanning the detuning frequency ω . Many different approximation methods could be used for that purpose. Since the displacement fields \bar{u}_i can be supposed continuous everywhere in the domain of definition and the

exact boundaries enclosing the solid medium can be rather arbitrary, a finite element model (FEM) is a natural choice. Our FEM is detailed in the appendix.

Once the displacement fields have been obtained, the full solution is known accurately. We find it useful to calculate the kinetic energy of the phonon wavepacket, as defined by

$$E_k = \frac{1}{4} \int_{\sigma} dr \rho \omega^2 \bar{u}_i(r)^* \bar{u}_i(r), \quad (5)$$

with ρ the material density and σ denoting the cross-section of the fiber. The elastic or potential energy is

$$E_p = \frac{1}{4} \int_{\sigma} dr \bar{u}_{i,j}(r)^* c_{ijkl} \bar{u}_{k,l}(r), \quad (6)$$

If the solution were a normal mode, then the elastic (or potential) energy would equal the kinetic energy. As the internal energy is the sum of kinetic and elastic energies, we estimate the phonon wavepacket energy as

$$E = E_k + E_p \approx 2E_k \quad (7)$$

with units J/m. We thus have access to both the Brillouin spectrum and the spatial distribution of three displacement components. Forward and backward interaction configurations can be considered, as well as any value of the k-vector. Contrary to the previous Brillouin models, the electrostriction force and hence the generated acoustic phonons are obtained right where the interaction takes place, without need to resort to a full band structure computation. As a consequence, our model can be universally applied to calculate the Brillouin gain characteristics with arbitrary refractive index and material compositions. In practice, and to allow for a fair comparison of deposited phonon wavepacket energies, the optical guided waves are normalized so that the flux of the z component of the Poynting vector is unity. This flux is

$$P_z = \text{Re} \left\{ \int_{\sigma} E^* \times H dS \right\}. \quad (8)$$

III. STRIP WAVEGUIDE

We consider a strip waveguide with lateral dimensions equal to $1.5 \mu\text{m}$ by $1 \mu\text{m}$, as depicted in Fig. 1(a). The solid core, made either of silicon (Si) or silica (SiO_2), is surrounded by air ($n = 1$). With these dimensions, the effects of radiation pressure are in principle almost negligible⁶. The different material constants used in the calculations are presented in Tab. I.

TABLE I. Independent material constants for silica and silicon.

Parameter	$n_{@1.55\mu\text{m}}$	ρ (kg/m ³)	p_{11}	p_{12}	p_{44}	c_{11} (GPa)	c_{12} (GPa)	c_{44} (GPa)	Qf (THz)
Si	3.47	2331	-0.10	-0.01	-0.051	166	64	79	50
SiO ₂	1.44	2203	0.12	0.27	-0.073	78	16	31	5

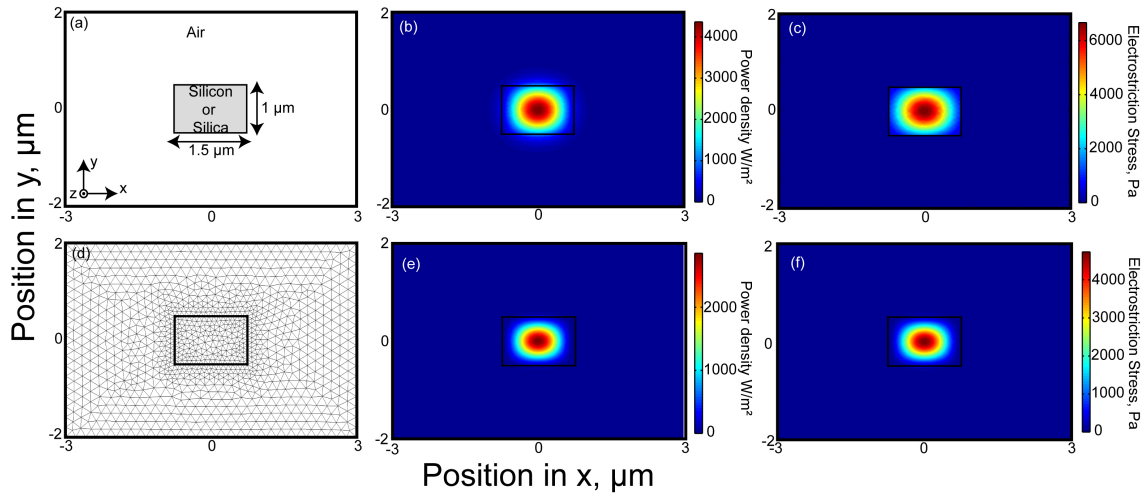


FIG. 2. (a) Cross section and (d) mesh of strip waveguide with lateral dimensions equal to $1.5 \mu\text{m} \times 1 \mu\text{m}$. Optical power density of the fundamental TE-like mode for $\lambda = 1550 \text{ nm}$ for (b) silica ($n_{\text{eff}} = 1.2748$) and (e) silicon ($n_{\text{eff}} = 3.3729$). Spatial distribution of electrostriction stress for (c) silica and (f) silicon.

The photoelastic coefficients for silicon at $1.5 \mu\text{m}$ have been extracted from Refs.^{16,17}. Here, p_{IJ} and c_{IJ} are the photoelastic and the elastic tensor presented in contracted notation¹⁸.

We first compute the optical guided waves using a 2D FEM model¹⁹. Fig. 2 displays the optical power density of the fundamental guided optical mode in the silica bridge for $\lambda = 1550 \text{ nm}$, for the cases of silica and silicon. The optical wavevector and the effective index of the mode are related by $k_1 = 2\pi n_{\text{eff}}/\lambda$. The resulting optical stress distributions are also shown in Fig. 2 and are seen to be smoothly varying functions reaching their maximum value at the center of the waveguide. The maximum stress is of the order of a few kPa for an incident optical power of 1 W.

To simulate the Brillouin interaction, elastic losses are incorporated in the electrostriction model by considering a complex elastic tensor $c_{ijkl} + i\omega\eta_{ijkl}$ where η_{ijkl} is a viscosity tensor²⁰.

This loss model is compatible with the usual assumption that the Qf product is constant for a given material. The symmetry of the viscosity tensor is the same as that of the elastic tensor. Viscosity constants are hardly available in the literature for silicon and silica. For silicon wafers, we estimated $Qf = 5.10^{13}$ Hz from independent experiments performed with bulk acoustic wave resonators. From measurements of the SBS linewidth in standard optical silica fiber, we estimated $Qf = 5.10^{12}$ Hz. So far, we have assumed that the loss factor for shear and longitudinal elastic waves is identical, but the model can consider a fully anisotropic viscosity tensor.

The elastic energy spectrum for forward and backward interaction in silica are presented in Fig. 3 and Fig. 4, and for silicon in Fig. 5 and Fig. 6. We superimpose on the elastic energy spectrum the discrete set of eigenfrequencies obtained without the optical force term, i.e., the phonon spectrum. The frequencies of elastic resonances calculated by our electrostriction model clearly match with a sub-set of eigenfrequency solutions, but with added information on the detailed spectral distribution of the Brillouin gain. In fact, the linewidth of elastic resonance and the efficiency of different elastic waves are clearly visible for both case.

A total of 8 selected phonon wavepacket distributions at resonance are shown in Figs. (3–6), labeled from A to H. In each case we have chosen to display the transverse displacement (defined as $\sqrt{u_1^2 + u_2^2}$), the axial displacement $|u_3|$, and the kinetic energy density. In the forward interaction case (A, B, E, F), displacements are purely transverse, and the elastic energy spectrum can be interpreted as a sum of Lorentzian resonances centered on eigenfrequencies of the waveguide. Resonances such as A, B, E, and F correspond to compressional modes of the rectangular resonator. Only a few of the eigenmodes are seen to be excitable by electrostriction of the symmetric optical stress distribution, as discussed by Rakich *et al.*⁶.

The backward interaction case (C, D, G, H), however, is quite different. Displacements are neither purely transverse or axial, but rather combine to form hybrid phonon wavepacket distributions²¹. Significantly, eigenfrequencies become very closely spaced as the frequency increases (especially in the case of Fig. 6), and become unresolvable at the scale of the Brillouin resonances. Consequently, resonances in the elastic energy spectrum cannot be thought anymore as corresponding to the broadening of one eigenfrequency, but rather correspond to the superposition of a finite number of eigenmodes. Such superpositions are especially apparent in phonon wavepacket distributions D and H, and result in interference

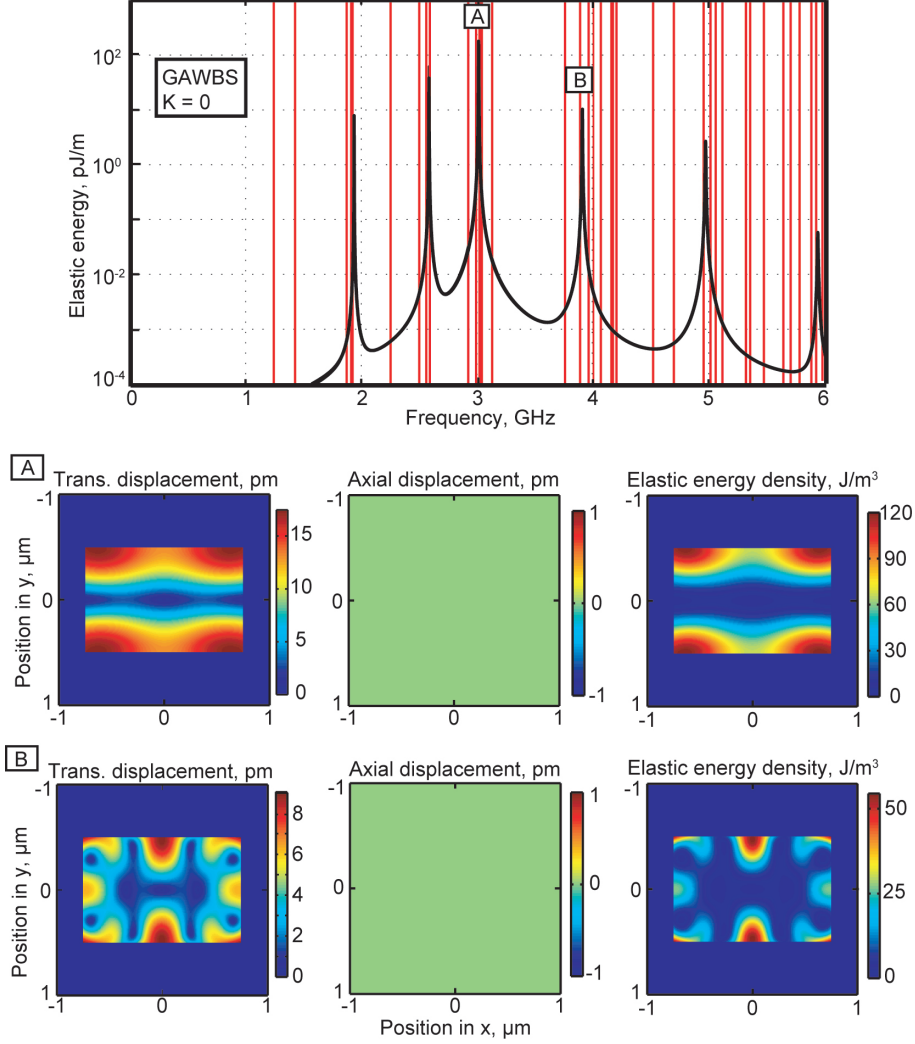


FIG. 3. Computed elastic energy as a function of frequency detuning ω for the silica strip waveguide in the forward (or GAWBS) configuration. The red vertical lines mark the eigenfrequencies of the acoustic problem. Spatial distribution of longitudinal and transverse displacements and kinetic energy density of resonant phonon wavepackets A (2.99 GHz) and B (3.89 GHz).

of the superposed eigenmodes. Elastic resonances D and H are directly related to the phase matching condition $k = 2k_1 = k_L$, where $k_L = \omega/c_L$ with c_L the longitudinal velocity in silica or silicon. This particular phase-matching leads to the usual SBS frequency formula $\omega_B/2\pi = 2n_{\text{eff}}c_L/\lambda$. In this case, axial displacements dominate the total deformation, but transverse displacements are still non vanishing.

In contrast, the total displacement of the elastic resonances C and G is dominated by transverse components. These phonon wavepacket distributions are mostly confined near the

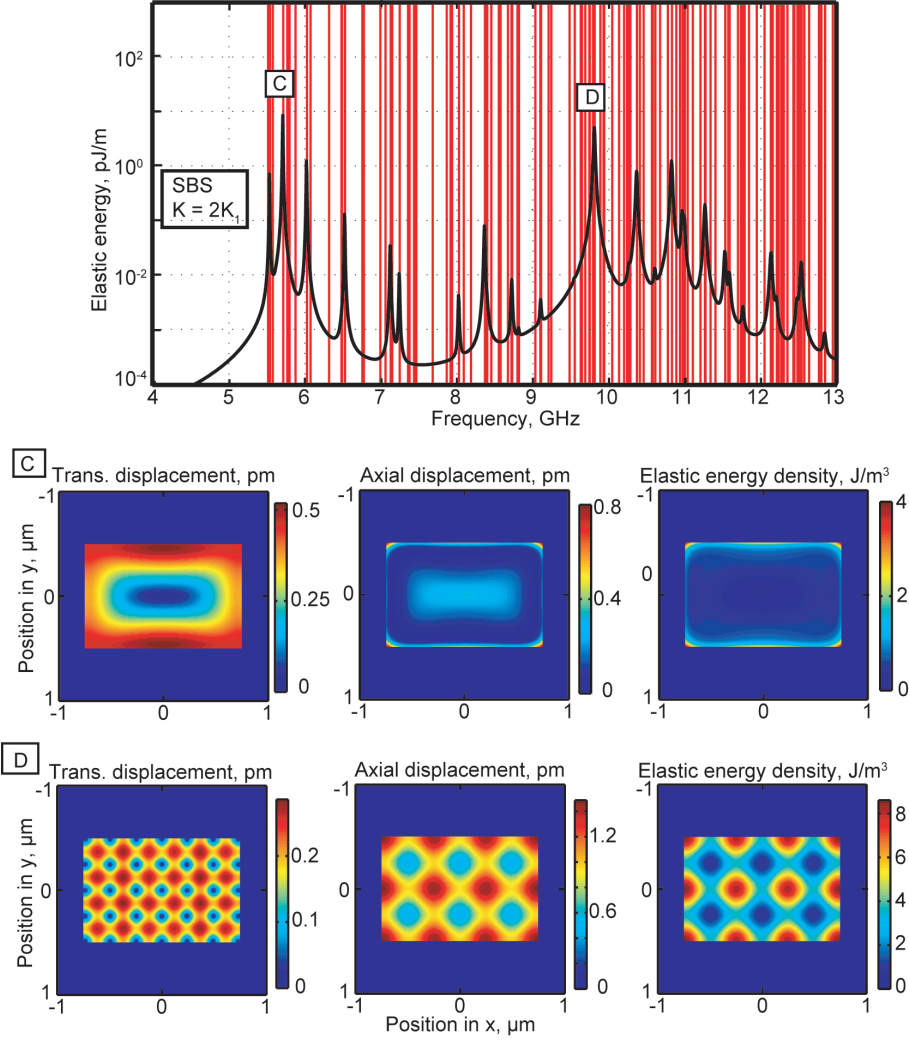


FIG. 4. Computed elastic energy as a function of frequency detuning Ω for the silica strip waveguide in the backward (or SBS) configuration. The red vertical lines mark the eigenfrequencies of the acoustic problem. Spatial distribution of longitudinal and transverse displacements and kinetic energy density of resonant phonon wavepackets C (5.71 GHz) and D (9.81 GHz).

boundaries of the waveguide, and can be loosely termed as surface guided phonon wavepackets, and the interaction is reminiscent of the case of Rayleigh surface waves overlapping with a guided optical mode of a planar waveguide²². This possibility is not found in standard silica optical fibers because the external boundaries are not close enough to the core of the waveguide.

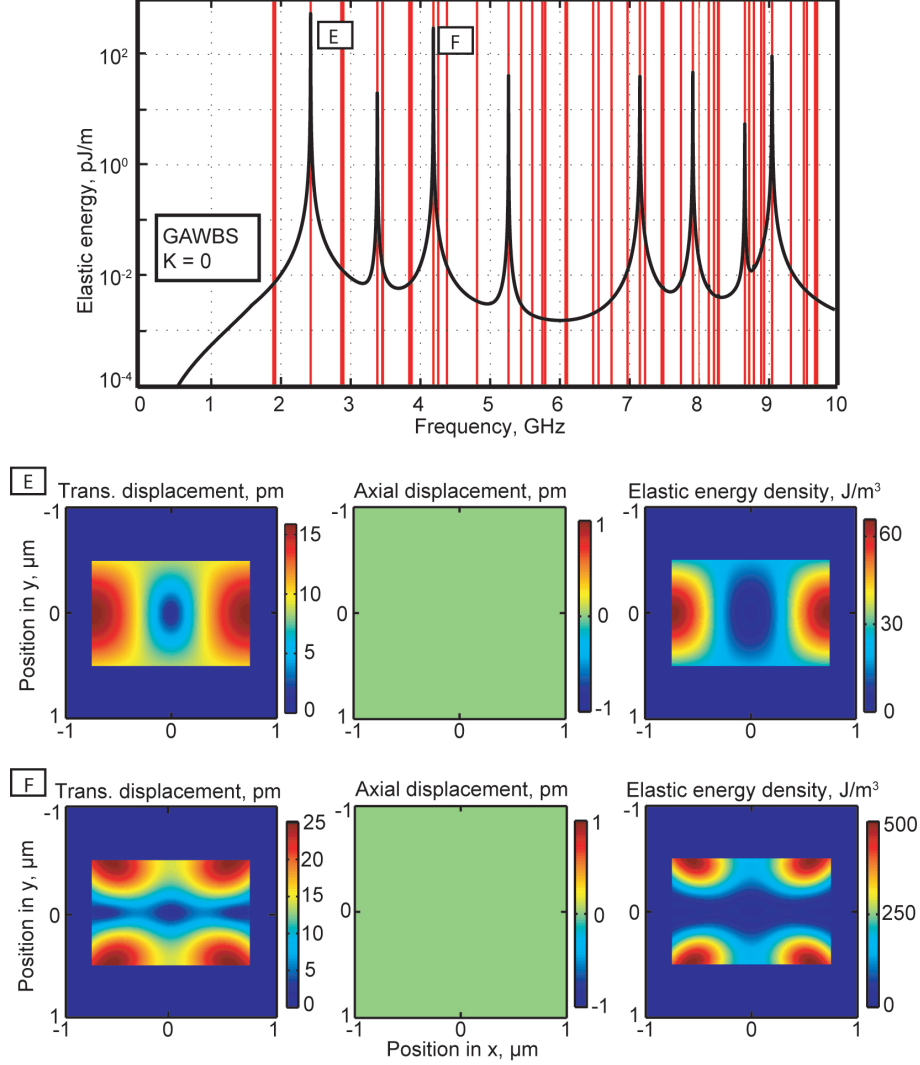


FIG. 5. Computed elastic energy as a function of frequency detuning ω for the silicon strip waveguide in the forward (or GAWBS) configuration. The red vertical lines mark the eigenfrequencies of the acoustic problem. Spatial distribution of longitudinal and transverse displacements and kinetic energy density of resonant phonon wavepackets E (2.48 GHz) and F = (4.24 GHz).

IV. DISCUSSION

A. Dependence of electrostriction efficiency with size

It was a major conclusion of Ref.⁶ that the gain of stimulated Brillouin scattering in silicon is strongly enhanced as the lateral size of the waveguide reduces down to approximately half a micron. We can derive from our model how the electrostriction gain scales with this

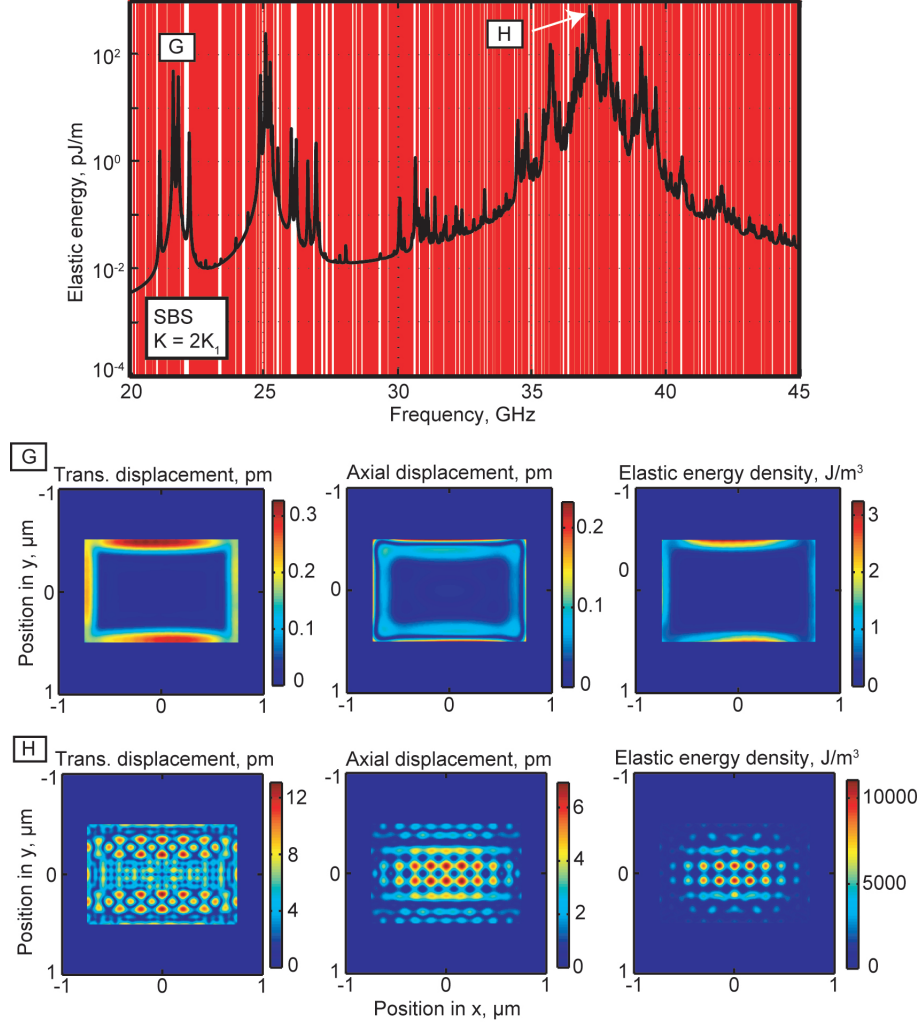


FIG. 6. Computed elastic energy as a function of frequency detuning Ω for the silicon strip waveguide in the backward (or SBS) configuration. The red vertical lines mark the eigenfrequencies of the acoustic problem. Spatial distribution of longitudinal and transverse displacements and kinetic energy density of resonant phonon wavepackets G (21.56 GHz) and H (37.2 GHz).

size. Quite naturally, a first source of enhancement comes from the choice to normalize the incident optical fields for unit transported power. As the same power has to be carried by a smaller cross-section, indeed, the electric field magnitude scales inversely with the size of the waveguide. As a result, the optical stress density scales with the inverse of the square of the size of the waveguide, as do the induced mechanical displacements, following Eq. (1). When the mechanical energy is integrated over the cross-section, the same square-inverse dependence is found for the electrostriction gain.

Apart from the straightforward normalization effect just discussed, it is natural to wonder

if there is an implied scale-dependence in the elastodynamic equation. Let us derive the corresponding energy statement. We denote the time-derivative of u_i by \dot{u}_i and consider a virtual displacement δu_i . Multiplying the equation by $\delta \dot{u}_i$, integrating over a volume V , and using Green's theorem (performing integration by parts), we arrive at

$$\frac{\partial}{\partial t} \left(\int_V dV \rho \delta \dot{u}_i \dot{u}_i + \int_V dV \delta u_{i,j} c_{ijkl} u_{k,l} \right) = \frac{\partial}{\partial t} \int_V dV \delta u_{i,j} T_{ij}^{\text{es}}. \quad (9)$$

This relation is analog to the theorem of virtual work in mechanics, as applied to work of the electrostriction stress. It is also equivalent to Poynting's theorem for elastic waves (when $\delta u_i = u_i$): Volume V is a cylinder with cross-section S and arbitrary length and the net flux of the elastic Poynting through both ends of the cylinder is zero; any variation of the internal elastic energy is proportional to the work of the electrostriction stress. According to relation (9), there is thus no obvious enhancement of electrostriction resulting simply from a reduction in the size of the waveguide. The boundary conditions obviously depend strongly on this size, however, and the solution to the elastodynamic equation will be quite strongly affected, including the elastic wave polarization. The energy transferred from optical waves to the phonon wave packet will be maximized with the work of the electrostriction stress, i.e., when the strain distribution $u_{i,j}$ matches the electrostriction stress T_{ij}^{es} pointwise. It is thus clear that there is some scale factor maximizing the electrostriction gain⁶.

B. Material constants

It comes as a surprise that the case of silicon seems to be favored over the case of silica in terms of electrostriction gain. Brillouin scattering in silica optical fibers is broadly documented and not too difficult to observe. With the photoelastic tensor written p_{IJ} in contracted notation, I and J being integers with values between 1 and 6, the literature generally attributes this fact to the rather large $p_{12} = 0.27$ value, that is favorable for longitudinal acoustic waves. In contrast, we are not aware of experimental results for silicon waveguides. In large core waveguides, the electric field is very nearly transverse. In small core waveguides as we consider, this assertion is not true anymore, but transverse components of the polarization still dominate. As a result, only values $J = 1, 2, \text{ or } 6$ have to be regarded among tensor components p_{IJ} . For both silica and silicon, there are 3 independent sets of constants. Let us discuss them separately.

TABLE II. Active photoelastic constants, and the polarization of the phonon wavepacket they give rise to, according to the interaction geometry.

Photoelastic constant forward backward		
$p_{11} = p_{22}$	L	S
$p_{31} = p_{32}$	–	L
$p_{12} = p_{21}$	L	S
p_{66}	S	S

First, of the set $p_{11} = p_{22} = p_{33}$, only p_{11} and p_{22} are active for elastic waves with S_1 and S_2 strain components, respectively. If we considered elastic plane waves, then only transverse longitudinal waves could be excited, but because of the transverse dependence of $u_1(r)$ and $u_2(r)$, strains S_1 and S_2 can be non vanishing even for axial shear elastic waves.

Second, the set $p_{12} = p_{13} = p_{23} = p_{21} = p_{31} = p_{32}$ implies two different cases. p_{31} and p_{32} couple to axial longitudinal elastic waves, as with stimulated Brillouin scattering in classical silica optical fibers. Note that in the case of silicon, $p_{12} = -0.01$ is very small and this coupling is not favoured. p_{12} and p_{21} would couple only to transverse longitudinal elastic waves if we were considering plane waves; as above, however, the transverse dependence of $u_1(r)$ and $u_2(r)$ generally allows coupling to axial shear elastic waves.

Third, of the set $p_{44} = p_{55} = p_{66}$, only p_{66} is active and creates a possibility for orthogonally polarized optical waves to generate phonons with non vanishing S_6 , corresponding to transverse shear waves only in the case of plane waves, but in addition to axial shear waves thanks to the transverse dependence of $u_1(r)$ and $u_2(r)$.

Table II summarizes the polarization of the phonon wavepackets that can be excited by each independent set of photoelastic constants. In the forward case, the axial wavevector k is always zero, meaning that elastic waves propagate in the (x_1, x_2) transverse plane. As a result, waves with $I = 1, 2$ are longitudinal (L) waves and waves with $I = 6$ are shear (S) waves²³. In the backward case, $k \neq 0$, and propagation is axial. As a result, waves with $I = 1, 2, 6$ are S waves and waves with $I = 3$ are L waves.

It is interesting to notice that the transverse dependence of axial displacement u_3 never enters the picture. Actually, this would require strains S_4 or S_5 to be active, through p_{44} or p_{55} , but these are excluded by the transverse hypothesis for the optical electric field. For

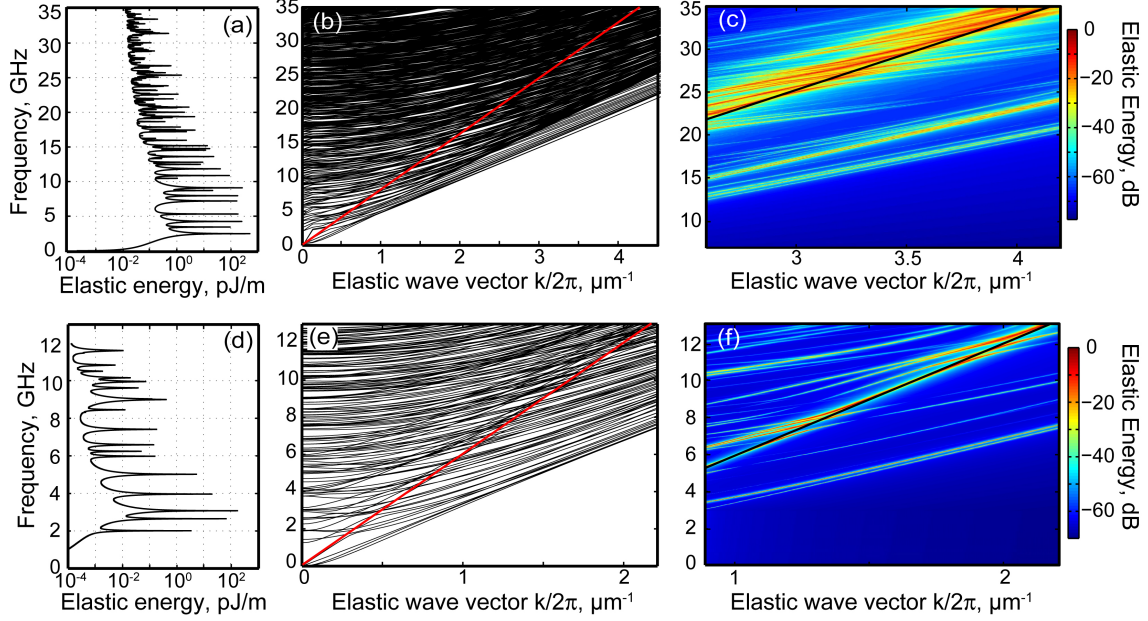


FIG. 7. (a) GAWBS and (b) SBS spectrum as a function of scale factor in silica bridge. For scale factor equal to 1, the GAWBS and SBS spectrum is presented in fig 2(a,b) respectively. For SBS configuration, the black line represents the phase matching condition ($k = 2k_1$). (a,d) GAWBS spectrum, (b,e) purely-acoustic dispersion diagram and (c,f) computed elastic energy as a function of elastic wave vector for silicon and silica, respectively. The red lines (b,d) and black lines (c,f) mark the phase matching condition $k = 2k_1$.

a fair comparison of silica and silicon, two additional facts have to be taken into account. First, χ_{ijkl} is n^4 times p_{ijkl} , which is a clear advantage for silicon. Second, the electrostriction gain is proportional to the Q-factor of the material¹²; since phonon loss is lower in silicon than in silica, this is again a clear advantage for silicon.

C. Phonon dispersion

The fact that the frequency detuning between the two optical waves can be scanned, on the one hand, and that the acoustic wavevector k is given by the difference of optical wavevectors in the backward interaction case, on the other hand, suggest that phonon dispersion can be probed all-optically. In this case, indeed, $k \approx 2k_1$ is almost independent of ω . Suppose that the frequency of a continuous wave laser can be adjusted to create a variable optical wavevector $k_1 = 2\pi n_{\text{eff}}(\lambda)/\lambda$, and that an electro-optical modulator is used

to shift the angular frequency of the second optical wave by ω . We have explicitly written $n_{\text{eff}}(\lambda)$ as a function of the wavelength, because of the dispersion of the optical waveguide. As a result, we would have access to any point $(\omega, k = k_1 - k_2)$ of the dispersion diagram for phonons. This is illustrated by Fig. 7. The central panels show the phononic band structure for silicon and silica. As we commented before, these band structures are densely populated. The corresponding elastic energy spectra at $k = 0$ (forward interaction) are shown in the left panels, and are essentially identical to the spectra shown in Fig. 3 and Fig. 5. The right panels show the elastic energy spectra for $k \neq 0$ (backward interaction), as obtained by varying both the optical wavelength and the frequency detuning. For each λ , the fundamental optical guided mode is computed and used to generate the elastic energy spectrum as a function of ω . Such a representation clearly shows the dispersion of electrostrictively active phonon wavepackets and their relation with phonon modes of the waveguide. An experimental arrangement as described above would give access to the dispersion of phonon wavepackets inside the optical waveguide, much as the technique of inelastic light scattering gives access to the dispersion of bulk, surface, or membrane phonons²⁴.

V. CONCLUSION

We have presented an electrostriction model for the generation of acoustic phonons in optical waveguides that is valid for an arbitrary spatial dependence of the optical field. We have identified the phonons that are excited in the forward and the backward interaction geometries and detailed their characteristics. Observing the spatial distribution of the generated phonon wave packets is of paramount importance in order to understand optoacoustic interactions under strong spatial confinement. It is found that small-core silicon waveguides seem to hold more potential than similar silica waveguides. The combination of large relative permittivity and high simultaneous confinement of photons and phonons explain the computation result. The computation method, i.e., solving the elastodynamic equation subject to an optical force, supersedes modal approaches in that it gives not only resonant frequencies but also the deposited phonon wavepacket energy, while at the same time accounting for viscoelastic damping. In our variational model, it would be interesting in the future to include optical forces of optomechanical origin, while only optical forces of electrostrictive origin have been considered so far. It has finally been suggested that phonon

dispersion in waveguides could be measured by all-optical means in the backward interaction geometry.

ACKNOWLEDGMENTS

This work was supported by the European program INTERREG IV (CD-FOM) and the European Community's Seventh Framework program (FP7/2007-2013) under grant agreement number 233883 (TAILPHOX).

Appendix A: Finite element model

In this appendix, we describe how a finite element model (FEM) can be derived from the elastodynamic equation subject to an electrostrictive force. We first obtain the fundamental guided optical mode from the hybrid-mode FEM formulation for electromagnetic waveguides¹⁹. Eqs. (3) and (4) are next inserted into (1)

$$-\rho\omega^2\bar{u}_ie^{-ikz} - (\bar{T}_{ij}e^{-ikz})_{,j} = -(\bar{T}_{ij}^{\text{es}}e^{-ikz})_{,j}, \quad (\text{A1})$$

with

$$\bar{T}_{ij}e^{-ikz} = c_{ijkl}(\bar{u}_ke^{-ikz})_{,l} \quad (\text{A2})$$

The displacement fields \bar{u}_i are assigned to live in a finite element space of Lagrange-type defined over the mesh of the waveguide cross-section. Free boundary conditions are applied. The elastic equation formulating a variational problem on the finite element space is obtained by left-multiplying by virtual displacement $(\bar{v}_ie^{-ikz})^*$ and integrating over the cross-section of the waveguide.

$$-\omega^2 \int_{\sigma} \rho \bar{v}_i^* \bar{u}_i - \int_{\sigma} (\bar{v}_i^* e^{ikz}) (\bar{T}_{ij} e^{-ikz})_{,j} = - \int_{\sigma} (\bar{v}_i^* e^{ikz}) (\bar{T}_{ij}^{\text{es}} e^{-ikz})_{,j}. \quad (\text{A3})$$

Next Green's theorem is used to transform integrals involving a divergence operator to integrals involving the gradient of the test function

$$\begin{aligned} & -\omega^2 \int_{\sigma} \rho \bar{v}_i^* \bar{u}_i + \int_{\sigma} (\bar{v}_i^* e^{ikz})_{,j} (\bar{T}_{ij} e^{-ikz}) - \int_{\delta\sigma} (\bar{v}_i^* e^{ikz}) ((\bar{T}_{ij} - \bar{T}_{ij}^{\text{es}}) e^{-ikz}) n_j \\ & = \int_{\sigma} (\bar{v}_i^* e^{ikz})_{,j} (\bar{T}_{ij}^{\text{es}} e^{-ikz}). \end{aligned} \quad (\text{A4})$$

The boundary integral is along $\delta\sigma$ and \mathbf{n} is the outward normal. The natural, or free, boundary condition is $\bar{T}_{ij}n_j = \bar{T}_{ij}^{\text{es}}n_j$ along $\delta\sigma$, meaning that the total normal stress vanishes on the boundary of the waveguide. Under this condition, the boundary integral vanishes. This weak formulation of the elastodynamic equation is all that is necessary for coding with a FEM language such as FreeFem++²⁵. Let us, however, provide more insight inside the structure of the FEM equations by expliciting the dependence with k

$$\begin{aligned} & \int_{\sigma} \bar{v}_{i,j}^* c_{ijkl} \bar{u}_{k,l} + ik \int_{\sigma} (\bar{v}_i^* c_{i3kl} \bar{u}_{k,l} - \bar{v}_{i,j}^* c_{ijk3} \bar{u}_k) + k^2 \int_{\sigma} \bar{v}_i^* c_{i3k3} \bar{u}_k - \omega^2 \int_{\sigma} \rho \bar{v}_i^* \bar{u}_i \\ & = \int_{\sigma} \bar{v}_{i,j}^* \bar{T}_{ij}^{\text{es}} + ik \int_{\sigma} \bar{v}_i^* \bar{T}_{i3}^{\text{es}}. \end{aligned} \quad (\text{A5})$$

Writing U and T^{es} the vectors of nodal values of the \bar{u}_i and the \bar{T}_J^{es} (in contracted notation), the usual Galerkin FEM procedure leads to the linear equations

$$(K + ikK_1 + k^2K_2 - \omega^2M)U = (X_0 + ikX_1)T^{\text{es}}. \quad (\text{A6})$$

Each of the matrices come from one of the integrals in Eq. (A5). The total stiffness matrix, $K = K + ikK_1 + k^2K_2$ is a polynomial of degree 2 in k . The mass matrix M is independent of the wavevector, as usual. The right-hand-side matrix $X = X_0 + ikX_1$, relating the optical force to the electrostriction stress, is a polynomial of degree 1 in k . In the forward interaction case, $k \approx 0$, and Eq. (A6) reduces to

$$(K - \omega^2M)U = X_0T^{\text{es}}. \quad (\text{A7})$$

In the backward interaction case, Eq. (A6) never simplifies except for large core waveguides: transversal strains can be neglected in this case and

$$(k^2K_2 - \omega^2M)U \approx ikX_1T^{\text{es}} \quad (\text{A8})$$

as a result. This is the short wavelength approximation that describes well SBS in classical silica optical fibers¹².

REFERENCES

- ¹T. P. M. Alegre, A. Safavi-Naeini, M. Winger, and O. Painter, [Opt. Express](#) **19**, 5658 (2011).

- ²V. Laude, J.-C. Beugnot, S. Benchabane, Y. Pennec, B. Djafari-Rouhani, N. Papanikolaou, J. M. Escalante, and A. Martinez, *Opt. Express* **19**, 9690 (2011).
- ³M. Eichenfield, J. Chan, R. M. Camacho, K. J. Vahala, and O. Painter, *Nature* **462**, 78 (2009).
- ⁴T. Kippenberg and K. Vahala, *Science* **321**, 1172 (2008).
- ⁵D. Van Thourhout and J. Roels, *Nature Photonics* **4**, 211 (2010).
- ⁶P. T. Rakich, C. Reinke, R. Camacho, P. Davids, and Z. Wang, *Phys. Rev. X* **2**, 011008 (2012).
- ⁷P. T. Rakich, P. Davids, and Z. Wang, *Opt. Express* **18**, 14439 (2010).
- ⁸A. Kobyakov, M. Sauer, and D. Chowdhury, *Adv. Opt. Photon.* **2**, 1 (2010).
- ⁹R. W. Boyd, *Nonlinear Optics*, 3rd ed. (Academic Press, 2008).
- ¹⁰A. H. McCurdy, *J. of Light. Tech.* **23**, 3509 (2005).
- ¹¹S. Dasgupta, F. Poletti, S. Liu, P. Petropoulos, D. J. Richardson, L. Grüner-Nielsen, and S. Herstrøm, *J. Lightwave Technol.* **29**, 22 (2011).
- ¹²J.-C. Beugnot and V. Laude, *Phys. Rev. B* **86**, 224304 (2012).
- ¹³V. Laude, A. Khelif, S. Benchabane, M. Wilm, T. Sylvestre, B. Kibler, A. Mussot, J. M. Dudley, and H. Maillotte, *Phys. Rev. B* **71**, 045107 (2005).
- ¹⁴R. Y. Chiao, C. H. Townes, and B. P. Stoicheff, *Phys. Rev. Lett.* **12**, 592 (1964).
- ¹⁵R. M. Shelby, M. D. Levenson, and P. W. Bayer, *Phys. Rev. B* **31**, 5244 (1985).
- ¹⁶D. K. Biegelsen, *Phys. Rev. Lett.* **32**, 1196 (1974).
- ¹⁷D. K. Biegelsen, *Phys. Rev. B* **12**, 2427 (1975).
- ¹⁸D. Royer and E. Dieulesaint, *Elastic waves in solids* (Wiley, New York, 1999).
- ¹⁹J. Jin, *The finite element method in electromagnetics, Second edition* (Wiley, New York, 2002).
- ²⁰R. P. Moiseyenko and V. Laude, *Phys. Rev. B* **83**, 064301 (2011).
- ²¹P. Dainese, P. S. J. Russell, N. Joly, J. Knight, G. Wiederhecker, H. Fragnito, V. Laude, and A. Khelif, *Nat. Phys.* **2**, 388 (2006).
- ²²R. N. Thurston, *J. Acoust. Soc. Am* **64**, 1 (1978).
- ²³Confusion should not be made between transverse propagation and shear waves, and axial propagation and longitudinal waves. We use the convention that longitudinal waves are characterized by the fact that deformations are in the direction of propagation; conversely, shear waves are characterized by the fact that deformations are orthogonal to the direction

of propagation.

²⁴J. Cuffe, E. Chávez, A. Shchepetov, P.-O. Chapuis, E. H. El Boudouti, F. Alzina, T. Kehoe, J. Gomis-Bresco, D. Dudek, Y. Pennec, B. Djafari-Rouhani, M. Prunnila, J. Ahopelto, and C. M. Sotomayor Torres, *Nano Letters* **12**, 3569 (2012).

²⁵<http://www.freefem.org/ff++/>.